Radiological characteristics study on epithelioid glioblastoma, a rare subtype of GBM

Xiaojuan Deng
Daping Hospital, Army Medical University
Qingya Luo
Southwest Hospital, Army Medical University
Xiaolin Tang
Daping Hospital, Army Medical University
Youqiang Chen
Daping Hospital, Army Medical University
Chengyi Mao
Daping Hospital, Army Medical University
Jingqin Fang (jingqin0405@163.com)
Daping Hospital, Army Medical University https://orcid.org/0000-0001-5521-1778

Research article

Keywords: Epithelioid glioblastoma. Radiological characteristics. Advanced MR. CT

Posted Date: July 3rd, 2019

DOI: https://doi.org/10.21203/rs.2.10915/v1

Abstract

Purpose Epithelioid glioblastoma (eGBM) is rare and a newly recognized subtype of GBM. Given the short of studies focusing on radiological characteristics of these tumors, we aimed to report the radiological features of eGBM deriving from six patients. Methods Six patients with pathologically diagnosed as eGBM were enrolled in this retrospective study. CT and pre-operative MR examinations with conventional and advanced sequences, such as diffusion weighted imaging and so on were analyzed. Immunohistological staining and mutation analysis of BRAF V600E was also explored. Results Only case 6 showed a co-locating tumor which was verified to be a diffuse astrocytoma (WHO II), other cases demonstrated single intracerebral tumor. Majority of the tumors originated in cerebral cortex, two cases involved corpus callosum. Tumors demonstrated iso-, hypo- or mixed intensity on T1WI, hyper- or mixed intensity on T2WI and FLAIR, heterogeneous enhancement on post-contrasted imaging. Involvement of leptomeninge, which appeared as leptomenigeal thickening and abnormal enhancing was discovered in 4 cases. Peritumoral edema (4/6) and hemorrhage (3/6) was common, calcium was only seen in case 5. Notable restrictive diffusion and consequently decreased rADC was found in solid component in 5 cases. Most cases demonstrated increased Cho and Lac/Lip value on 1H-MRS, and promoted rCBV value on PWI. The cases with CT examination showed an ill-defined mass with mixed density. Conclusions Although there are some overlaps between typical GBM and eGBM, some radiological characteristics, such as location (often in cerebral cortex), involvement of leptomeninge and intratumoral calcium, may support the diagnosis of eGBM.

Background

Glioblastoma (GBM), the most common and devastating tumor in central nervous system(CNS) of adult, has a very poor prognosis in despite of intensive treatment. Epithelioid glioblastoma (eGBM), firstly describing as “closely packed tumor cells arranged in sold trabeculae and club-like formations” [1], is formally identified as an entire subtype of GBM in 2016 World Health Organization (WHO) classification of CNS. Due to its early recurrence, rapid progression and dissemination (leptomeninge and cerebrospinal fluid), eGBM display more aggressive clinical course and with a median survival time shorter than 14.5 months in typical GBM [2].

The etiology and cell origin of eGBM remain unknown. Although in several cases, a low grade astrocytoma or pleomorphic xanthoastrocytoma (PXA) has found to be as pre-existing or co-existing lesion with an eGBM, eGBM is usually recognized as a *de novo* neoplasm according to the presence of wild type isocitrate dehydrogenase 1 (IDH-1) and absence of ATRX mutation. To date, only one case is diagnosed as a secondary eGBM with IDH-1 mutation that develop from a oligoastrocytoma (WHO grade II) [3]. There is a close relationship between the eGBM and PXA since those two types of tumor share high overlap of genetic alteration, such as serine/threonine kinase B-Raf (BRAF) V600E mutation and TERT promoter (*TERT-p*) mutation. Even some authors propose that eGBM may arise from a PXA with BRAF V600E mutation [4].

Owing to insufficient recognition resulting from its rarity and intratumoral heterogeneity of eGBM, making an exact diagnosis encounter huge challenge. In the current study, we collected 6 cases initially diagnosed as eGBM. Of particular note, one case had a co-locating diffuse astrocytoma (WHO grade ii), both of that two tumors harbored IDH-1 mutation. In our knowledge, that case is the second eGBM case displaying IDH-1 mutation. In order to help making a more accurate diagnosis, this study was more on discovering radiological characteristics of eGBM. Beyond that, we described and analyzed clinical and histological features of the 6 cases.

Methods

For retrospective analysis, consecutive 6 patients who were pathologically diagnosed as epithelioid glioblastoma (eGBM) were enrolled. 4 cases were male, 2 were female, aged from 18-year to 52-year, the median age was 35.5 years. Durations of the clinical symptoms varied from several days to 1 year. Prior to any treatment, all the cases performed conventional MR scanning with or without contrast agent, diffusion-weighted imaging (DWI), susceptible-weighted imaging (SWI) and ^{1}H-MR spectroscopy (^{1}H-MRS). Moreover, 4 cases undertook dynamic susceptibility contrast-enhanced perfusion weighted imaging (DSC-PWI). 3 cases accepted plaint and enhanced CT scan.

This study was approved ethically by the institutional review board at Daping Hospital, Army Medical University (Chongqing, China) (IRB #201879). All the patients with suspected glioma had previously informed the possibility of using their medical imaging for research and obtained authorization for utilization of their medical records.

2.1 Radiological scanning protocol

All patients performed conventional and advanced MR scanning on a 3.0T MR scanner (Verio, Siemens, Erlangen, Germany), with an 8-channel head coil. Conventional MR imaging included following sequence: turbo spin-echo T2-weighted images (T2WI, TR/TE 4900/96ms, number of excitations, NEX 1), T2-weighted fluid-attenuated inversion-recovery (FLAIR, TR/TE 8000/94ms, NEX 1), pre-contrast gradient-echo T1-weighted images (T1WI, TR/TE 440/2.48ms, NEX 1) and post-contrast T1WI with identical parameters used in pre-contrast T1WI scanning. All the images were acquired with a field of view (FOV) of 230×230mm^2 and 24 axial slices of 5mm with intersection space of 1mm. The contrast agent Gd-DTPA (magnevist solution, Guangzhou Consun Pharmaceutical Co., Ltd, Guangzhou, China) was injected at a dose of 0.2mmol/kg of body weight and rate of 3-4ml/s. DWI was performed prior to T1WI with contrast, using an echo planar imaging (EPI) sequence, TR/TE 6600/100ms, b-value (0, 600, 1000), FOV230×230mm^2. Apparent diffusion coefficient (ADC) maps were acquired using an images post-processing software (Siemens syngo, Siemens, Erlangen, Germany). DSC-PWI was performed using a SE-EPI sequence with following parameters: TR/TE 1872/30ms, flip angle 90°, NEX 1.0, matrix 128×128, FOV 230×230mm^2. For each section, 20 images were obtained. After acquiring the 6th image, a bonus of Gd-DTPA at a dose of 0.2mmol/kg was injected at a rate of 3-4ml/s, immediately following by a bonus of equivalent dose of saline. The parameters of ^{1}H-MRS (2D multi-voxel chemical shift imaging, CSI) were as follows: TR/TE 1700/135ms, FOV 160×160mm^2, voxel thickness 10mm, NEX 3.0, FWHM<20HZ. The regions of interest (ROI) covered tumorous solid area, periphery region of tumor and contralateral normal

region. SWI was performed using a 3D multi-echo flow compensated GRE sequence with the following parameters: TR/TE 27/20ms, flip angle 10°, FOV 200 × 200 mm^2, matrix 256 × 182, slice thickness 1.5 mm, scan range 135 mm.

CT was performed on a 64-slice CT scanner (LightSpeed VCT, GE healthcare, Milwaukee, WI). The parameters were as follows: tube voltage 120KV, tube current 350mA, slice thickness 5mm, matrix 512×512, FOV 9.6cm. After plain CT, the iodine contrast agent (Ultravist, Bayer Healthcare, Leverkusen, Germany; 370mg/ml) at a dose of 300mg/kg was administrated via an automatic switching injector (Ulrich medical, Ulm, Germany) at a speed of 3.5ml/s.

2.2 Imaging post-processing and analysis

All the DSC-PWI and DWI original data were processed with a commercial post-processing software package (SygnoMMWP VE36A, Siemens, Erlangen, Germany) to obtain cerebral blood volume (CBV) and ADC maps. The imaging analysis was performed by two experienced, board-certified neuro-radiologist with more than 5-year work experience. The ROIs with identical size were placed on the solid component and contralateral normal appearance white matter (NAWM), CBV_{max} and ADC_{min} was determined. Then, the $rCBV_{max}$ and $rADC_{min}$ were calculated by normalizing CBV_{max} and ADC_{min} to the value of contralateral NAWM. On ^{1}H-MRS, Lip/Lac value was stratified: -, totally negative or can't be measured; 1+, detectable; 2+, the second peak; 3+, the largest peak [5]. According to the method provided by Park et al. [6], intratumoral susceptibility signal intensity (ITSS) on SWI was scored as follows: 0, absent; 1, number of ITSS $\leq$ 5; 2, ITSS $\leq$ 10; 3, ITSS $\geq$ 11.

2.3 HE and immunohistological staining

HE staining was performed on 4μm sections of formalin-fixed paraffin-embedded (FFPE) specimens. Immunohistological staining was done following EnVision kit specification and using antibodies against glial fibrillary acidic protein (GFAP), Nestin, IDH-1, Olig-2, p53, NeuN, S-100, integrase interactor 1 (INI-1), Syn, CD34 and Ki-67. All the primary antibodies were brought from MXB (MXB Biotechnology Co, Fuzhou, China).

2.4 Mutation analysis of BRAF V600E

DNA was extracted from the paraffin-embedded specimens by using DNA extraction Kit (Amoy Diagnostics, Xiamen, China) and following the manufactural protocol. *BRAF* V600E ARMS-PCR Kit (Amoy Diagnostics, Xiamen, China) was applied to determine the mutation statue of the specimens, all the procedures followed the kit specification.

The total reaction system was 45μL, including 5μL DNA template and 40μL reaction mixture (consist of Taq DNA polymerase, scorpions primer, reaction buffer and so on). Each reaction contained a positive and a negative control. The PCR reaction was performed as follows: Stage i 95℃for 5min; Stage ii 95℃for 25s followed 72℃for 20s, repeated 15 cycles; Stage iii 93℃ for 25s, 60℃ for 35s, 72℃ for 20s, repeated 31 cycles. Data was automatically collected when the reaction was completed. Mutation result was concluded based on the manufacture instruction.

Results

3.1 Clinical characteristics

The clinical symptoms depended on the location of the tumor, predominantly presented symptoms associated with intracranial hypertension including dizzy, headache and vomiting (5/6). One case demonstrated convulsion of the limbs accompanying conscious disturbance (1/6). All lesions located in supratentorial region. 3 cases were primary tumor, 2 were recurrent tumor, 1 was co-located with a diffusion astrocytoma. All cases underwent surgical resection, the post-operative radiotherapy and chemotherapy with temozolomide was applied in 3 cases. 1case died soon after surgery, 1 missed the follow-up data, the other 4 cases were alive until June 2018. (Table 1) Survival time ranged from 11 to 22 months, average survival time was 14.7 months.

3.2 Radiological features

Among the 6 cases, only case 6 co-located with a low-grade glioma (Fig 1), both the other 5 cases were single tumor. 5 cases originated in cerebral cortex involving temporal (3/6) and frontal lobes (2/6), 1 developed in basal ganglia and corpus callosum. Cerebrospinal fluid (CSF) dissemination was noted in one case. The tumors displayed massive (4/6) or irregular (2/6) growth pattern, 5 cases presented solid with cystic appearance, and 1 case showed pure solid appearance. The average maximum diameter of the tumors was 5.3cm (3.3~6.8cm). Most cases showed a relatively well-circumscribed lesion (4/6), 2 cases were ill-defined (2/6). Mild (case 1, 2) or severe (case 5, 6) peritumoral edema was noted, absence of peritumoral edema was found in the other 2 cases. Intratumoral necrosis (4/6), hemorrhage (3/6) and calcification (1/6) also was detected.

On conventional MRI, tumors presented iso-and hypointensity (3/6) or mixed intensity (3/6) on T1WI, mild hyperintensity (3/6) or mixed intensity (3/6) on T2WI and FLAIR (Fig 2a-c). With contrast agent, majority tumors (5/6) demonstrated markedly heterogeneous enhancement with both cystic wall and solid component exhibiting striking enhancing, only one case showed slight enhancement (Fig 2d). Notably, case 4 revealed area with nodular-enhancing pattern within the tumor. Moreover, linear and patchy enhancement was observed in tentorium cerebelli and superior vermis of cerebellum in case 4, that indicated a CSF dissemination (Fig 3). Involvement of leptomeninge was discovered in 4 cases showing leptomeningeal thickening and abnormal enhancing (Fig 2d). All 6 cases performed DWI and obtained $rADC_{min}$ via image post-processing, 5 cases revealed notable restricted-diffusion within the solid component of the tumor (Fig 4a-b), only 1 case (case 3) showed mild restricted-diffusion which may be attributed to the influence from the skull base near the tumor. The $rADC_{min}$ values of the tumor were decreased, the average value was 0.84×10^{-3} mm^2/s (0.78×10^{-3} ~ 0.93×10^{-9} mm^2/s). SWI was not available in case 6, dotted or patchy hypointensity was noted within the other cases (Fig 4c). According to the grading method mentioned above, the 5 cases can be divided into 0 (case

3), 1 (case 5), 2 (case 1) and 3 (case 2 and 4). On ^{1}H-MRS, except case 3, whose baseline was unstable resulting from the influence of adjacent skull base, the other 5 cases demonstrated decreased NAA, increased Cho value and Cho/NAA ratio, the average Cho/NAA value was 12.94 (3.6 ~ 33.2). Increased Lac/Lip value also can be found in case 1, case 2, case 4 and case 6 with grade 2+, 1+, 1+ and 2+, respectively (Fig 4d). For 4 cases (case 2, 4, 5 and 6) with DSC-PWI examination, all without exception presented increased rCBV, the $rCBV_{max}$ differed from 4.44 to 7.55, the mean $rCBV_{max}$ was 5.94 (Fig 4e).

On CT, all the cases (case 2, 4 and 5) showed an ill-defined mass with mixed density. Solid component exhibited higher density compared to the contralateral normal brain, while cystic area within the tumor exhibited low density. The CT images also clearly exhibited the intratumoral hemorrhage and calcification.

3.3 Histopathological findings

The tumors were consisted by epithelioid tumor cells which were round or oval, abundant eosinophilic cytoplasm, overt nuclei and mitotic figures, sometimes with intranuclear pseudoinclusions (Fig 5a). Multinucleated giant cells were found in some cases. All the cases revealed necrosis showing geographic or pseudo-palisading pattern. Local spindle cells with sarcomatoid change was seen in case 5 (Fig 5b). The spindle cells showed obvious atypia, intensive cellular proliferation and transition zone, which made a distinction between spindle cells and epithelioid tumor cells. Stromal vascular proliferation was evident. Glomeruli-like vessels were seen in periphery area of tumor necrosis and hyperplastic stromal vessels.

All cases showed positive GFAP, p53 and Syn staining with variable immunoreactivity. Sevaral cases showed variable immunopositivity (5/6) for S-100, Nestin and Olig-2 (4/6). Positive INI-1 staining was seen in all cases (Fig 5c-e). In case 6, IDH-1 mutation was found both in eGBM and co-existing low grade diffuse astrocytoma region (Fig 5f-g). Ki-67 labeling index varied among 20% to 30%.

BRAF V600E mutation, which is less frequently found in other types of GBM, can be found in eGBM at a relatively high frequency of 56%. In our six cases, three cases (50%) harbored BRAF V600E mutation (Fig 5h).

Discussion

Since eGBM is a newly recognized subtype of GBM according to criterion of the latest WHO classification (2016), a large cohort is hard to obtain. To date, only Korshunov A, et al. reported a series of sixty-four cases [7]. Therefore, the incidence rate of eGBM is not available. Due to its rarity, reported cases pay more attention to the histological and clinical features of eGBM rather than radiological findings. To date, only one case of eGBM with IDH-1 mutation is reported [3], although several cases report eGBM with pre-exiting or co-exiting tumor, such as PXA or low-grade diffuse astrocytoma [3, 4, 8-11]. In the present study, we reported one eGBM collocating with a low-grade diffuse astrocytoma, and in that two tumor districts, IDH-1 instead of BRAF V600E mutation was found. Moreover, we summarized and analyzed clinical, MRI/CT and histological features of six cases. The radiological findings, especially the findings obtained from the advanced MR sequences was the key attention of this study.

Unlike typical GBM tend to occur in elderly people, eGBM apt to afflict children and young adults at less than 30 years old [12, 13]. eGBM usually arise in cerebral cortex and diencephalon. In adult, eGBM often develop predominantly in cerebral cortex, temporal and frontal lobe are the most common locations. While, pediatric eGBM commonly occur in diencephalon [14]. Age at initial diagnosis of this study was disagree with previous reports, only 2 in 6 cases of this study were young people at less than 20 years old, the other 4 cases ranged from 30 to 50 years old. This discrepancy suggests that eGBM may be with a wider age spectrum. There was no gender prevalence, the ratio of male versus female was 1:1 (3/3). Consistent with the reported studies, 3 cases (50%) located in temporal lobe, 2 out 6 cases involved frontal lobe, 1 case occurred in basal ganglia region. However, 2 cases (case 4, 6) involved deep brain structure, including corpus callosum and basal ganglia. That may indicate the heterogeneity of eGBM just like typical GBM. The common complications, like headache (4/6), may be intracranial hyperintension associated.

BRAF V600E mutation is found in several types of CNS tumors, including PXA, PXA with anaplasia, gangliogliomas, anaplastic gangliogliomas and extra-cerebellarpilocyticastrocytomas [10]. Recently, a 64-cases cohort study demonstrates up to 56% eGBM can be detected BRAF V600E mutation, while this mutation is rarely found in other types of GBM [7]. BRAF V600E mutation state constitutively activates MAPK signaling pathway, which lead to the increasing of cell proliferation, apoptosis resistance and tumor progression. That may explain the more aggressive phenotype of eGBM. In the six cases reported here, BRAF V600E mutation was observed in three cases (50%) and thus coincided with the previous reports. As expected, all six cases were immunoreactive for INI-1, the focal loss of which used to be proposed as a valuable marker to identify eGBM from rhabdoid GBM [15]. However, with increasing INI-1-immunoreactive rhabdoid GBMs (rGBM) are identified, the distinguishing value of IN1-1 between eGBM and rhabdoid GBM is doubtable. IDH-1 mutation, which is often seen in secondary GBM, is uncommon to be found in eGBM. To our knowledge, besides the case 6 in this study, there is only one previously reported eGBM case with IDH-1 mutation. That reported eGBM with IDH-1 mutation is progressed from a mixed oligoastrocytoma (WHO grade II) in the resected cavity. While, in the current presentation, the case 6 was concurrent with a WHO-II diffuse astrocytoma. Taken together, those findings suggest that BRAF V600E mutation may play a vital role in tumorigenesis of eGBM. In addition, other genetic alterations including IDH-1 mutation in the context of BRAF V600E mutation could result in transformation of a low-grade glioma into eGBM.

Radiologically, eGBM mostly showed cystic and solid appearance with mass or irregular configuration. Like the typical GBM, moderate or severe peritumoral edema, necrosis and hemorrhage was commonly seen in all cases of this study. Invasion into the wall of vessels in the subarachnoid space and discohesiveness of tumor cells may be related to the extensive intratumoral hemorrhage of eGBM [12]. Calcium, which is remotely found in typical GMB, is often detected in eGBM with pre-exiting or co-exiting lesion. Therefore, calcium is supposed to accompany with secondary eGBM [16]. To our surprise, CT detected calcium in case 4, which was a primary eGBM. That finding may suggest that calcium can present both in original and secondary eGBM, and may exert distinguishing value between typical GBM and eGBM. Involvement of leptomeninge and cerebrospinal fluid dissemination are notable characteristics of eGBM, most reported cases refer to that. Frequently locating in cerebral cortex may contribute to the invasion of leptomeninge, which demonstrate thickening and aberrant enhancement with contrast medium. In the current study, three cases revealed an abnormal enhancement of leptomeninge, but only one case

showed a “dura matter tail” sign. In addition, case 4 broke through the basal ganglia resulting in dissemination in lateral ventricle, vermis and tentorium of cerebellum at diagnosis. Advanced MR sequence can supply more detailed information associate with cellularity, vascular dynamics, tumoral metabolism and so on. Similar to high grade glioma, eGBM exhibited a markedly restricted diffusion on DWI, increased Cho/NAA ratio on ^{1}H-MRS and $rCBV_{max}$ value on DSC-PWI. Owing to intratumoral hemorrhage or calcium, diffusely patchy or dotted hypointensity which was ranked grade 2 or 3, was found on SWI in 3 cases.

Conclusions

In summary, eGBM is a newly recognized subtype of GBM until 2016 WHO classification of CNS tumor, the more specific features including clinical, radiological and histopathological remains further study. Although radiological features have some overlaps between typical GBM and eGBM, some characteristics, such as location (often in cerebral cortex), involvement of leptomeninge, intratumoral calcium, may support the diagnosis of eGBM. In addition, young patient has a history of PXA or low grade glioma with BRAF V600E mutation should be hypervigilant for transformation into eGBM.

Abbreviations

Cho, Choline; CNS, central nervous system; CSF, cerebrospinal fluid; CT, computed tomography; DWI, diffusion weighted imaging; DSC-PWI, dynamic susceptibility contrast-enhanced perfusion weighted imaging; eGBM, Epithelioid glioblastoma; FLAIR, fluid-attenuated inversion-recovery; FOV, field of view; GBM, glioblastoma; GFAP, glial fibrillary acidic protein; IDH-1, isocitrate dehydrogenase 1; INI-1, integrase interactor 1; ITSS, intratumoral susceptibility signal intensity; Lac, lactate; Lip, lipid; MRS, magnetic resonance spectroscopy; NAA, N-acetylaspartate; ROI, region of interest; SWI, susceptible-weighted imaging; T1WI, T1 weighted imaging; T2WI, T2 weighted imaging; PXA, pleomorphic xanthoastrocytoma; rADC, relative apparent diffusion coefficient; rCBV, relative cerebral blood volume

Declarations

Ethics approval and consent to participate

This study was approved by the institutional review board at Daping Hospital, Army Medical University (IRB #201879), and all procedures performed in studies involving human participants were in accordance with the ethical standards of the institutional research committee. Written informed consent was obtained from all the patients.

Consent for publication

Written informed consent from study participant for publication of their cases and accompanying images.

Availability of data and materials

The datasets used and/or analyzed during the current study are presented within the manuscript as table and figure, and all the radiological figures are available from the corresponding author on reasonable request.

Competing interests

Not applicable

Funding

Not applicable

Authors' contributions

All the authors have read and approved the manuscript. JQF designed the study and made the revisions; XJD wrote the manuscript; QYL analyzed pathological figures and BRAF V600E mutation; XLT analyzed and summarized the radiological features; YQC collected radiological figures of the cases; CYM collected pathological figures.

Acknowledgements

Not applicable

References

1. Rubinstein LJ. The development of contiguous sarcomatous and gliomatous tissue in intracranial tumours. J Pathol Bacteriol. 1956;71:441-59.
2. Sugimoto K, Ideguchi M, Kimura T, Kajiwara K, Imoto H, Sadahiro H, Ishii A, Kawano H, Ikeda E, Suzuki M. Epithelioid/rhabdoid glioblastoma: a highly aggressive subtype of glioblastoma. Brain Tumor Patho. 2016;l33:137-46.
3. Kleinschmidt-DeMasters BK, Aisner DL, Birks DK, Foreman NK. Epithelioid GBMs show a high percentage of BRAF V600E mutation. Am J Surg Pathol. 2013;37:685-98.
4. Tanaka S, Nakada M, Nobusawa S, Suzuki SO, Sabit H, Miyashita K, Hayashi Y. Epithelioid glioblastoma arising from pleomorphic xanthoastrocytoma with the BRAF V600E mutation. Brain Tumor Pathol. 2014;31:172-6.

5. Park MJ, Kim HS, Jahng GH, Ryu CW, Park SM, Kim SY. Semiquantitative assessment of intratumoral susceptibility signals using non-contrast-enhanced high-field high-resolution susceptibility-weighted imaging in patients with gliomas: comparison with MR perfusion imaging. AJNR Am J Neuroradiol. 2009;30:1402-8.
6. Yamasaki F, Takayasu T, Nosaka R, Amatya VJ, Doskaliyev A, Akiyama Y, et al. Magnetic resonance spectroscopy detection of high lipid levels in intraaxial tumors without central necrosis: a characteristic of malignant lymphoma. J Neurosurg. 2015;122:1370-9.
7. Korshunov A, Chavez L, Sharma T, Ryzhova M, Schrimpf D, Stichel D, et al. Epithelioid glioblastomas stratify into established diagnostic subsets upon integrated molecular analysis. Brain Pathol. 2018;28:656-62.
8. Chi AS, Batchelor TT, Yang D, Dias-Santagata D, Borger DR, Ellisen LW, Iafrate AJ, Louis DN. BRAF V600E mutation identifies a subset of low-grade diffusely infiltrating gliomas in adults. J Clin Oncol. 2013;31:e233-6.
9. Nobusawa S, Hirato J, Kurihara H, Ogawa A, Okura N, Nagaishi M, Ikota H, Yokoo H, Nakazato Y. Intratumoral heterogeneity of genomic imbalance in a case of epithelioid glioblastoma with BRAF V600E mutation. Brain Pathol. 2014;24:239-46.
10. Kuroda J, Nobusawa S, Nakamura H, Yokoo H, Ueda R, Makino K, Yano S, Kuratsu J. A case of an epithelioid glioblastoma with the BRAF V600E mutation colocalized with BRAF intact low-grade diffuse astrocytoma. Neuropathology. 2016;36:181-6.
11. Funata N, Nobusawa S, Yamada R, Shinoura N. A case of osteoclast-like giant cell-rich epithelioid glioblastoma with BRAF V600E mutation. Brain Tumor Pathol. 2016;33:57-62.
12. Nakajima N, Nobusawa S, Nakata S, Nakada M, Yamazaki T, Matsumura N, Harada K, et al. BRAF V600E, TERT promoter mutations and CDKN2A/B homozygous deletions are frequent in epithelioid glioblastomas: a histological and molecular analysis focusing on intratumoral heterogeneity. Brain Pathol. 2018;28:663-73.
13. Sugimoto K, Ideguchi M, Kimura T, Kajiwara K, Imoto H, Sadahiro H, Ishii A, et al. Epithelioid/rhabdoid glioblastoma: a highly aggressive subtype of glioblastoma. Brain Tumor Pathol. 2016;33:137-46.
14. Broniscer A, Tatevossian RG, Sabin ND, Klimo P Jr, Dalton J, Lee R, Gajjar A, Ellison DW. Clinical, radiological, histological and molecular characteristics of paediatric epithelioid glioblastoma. Neuropathol Appl Neurobiol. 2014;40:327-36.
15. Kleinschmidt-DeMasters BK, Alassiri AH, Birks DK, Newell KL, Moore W, Lillehei KO. Epithelioid versus rhabdoid glioblastomas are distinguished by monosomy 22 and immunohistochemical expression of INI-1 but not claudin 6. Am J Surg Pathol. 2010;34:341-54.
16. Nitta N, Moritani S, Fukami T, Yoshimura Y, Hirai H, Nozaki K. Intraventricular Epithelioid Glioblastoma: A Case Report. World Neurosurg. 2018;112:257-63.

Tables

Table 1 Clinic characteristics and MRI features

Case	Case 1	Case 2	Case 3	Case 4	Case 5	Case 6
Age	32	46	19	18	52	46
Gender	Male	Male	Female	Female	Male	Female
Presentation	Headache	Headache	Convulsion of the limbs	Palpitation	Headache	Headache and dizzy
Location	Left temporal lobe	Right temporal lobe	Left temporal lobe	Left basal ganglia and splenium of corpus callosum	Right frontal lobe	Bilateral frontal lobe and genu of corpus callosum
Examination protocols	cMRI/DWI/SWI/MRS	cMRI/DWI/SWI/ MRS/PWI CT	cMRI/DWI/SWI/MRS	cMRI/DWI/SWI/MRS/PWI CT	cMRI/DWI/SWI/MRS/PWI CT	cMRI/DWI/SWI/MRS/PWI
MRI features						
border	Well-defined	Ill-defined	Well-defined	Ill-defined	Well-defined	Well-defined
periphery edema	Mild	Mild	-	-	Severe	Severe
leptomeninges involvement	-	+	+	+	+	-
necrosis	+	+	-	-	+	+
hemorrhage	+	+	-	+	-	-
calcium	-	-	-	-	+	-
DWI	Severe	Severe	Mild	Severe	Severe	Severe
SWI	2	3	0	3	1	NA
Cho/NAA	33.2	4.7	NA	8.5	3.6	7.2

Abbreviations: cMRI, conventional MRI; DWI, diffusion weighted imaging; SWI, susceptible-weighted imaging; MRS, ^{1}H-MR spectroscopy; PWI, perfusion weighted imaging. NA, not available. +, presence; -, absence

Figures

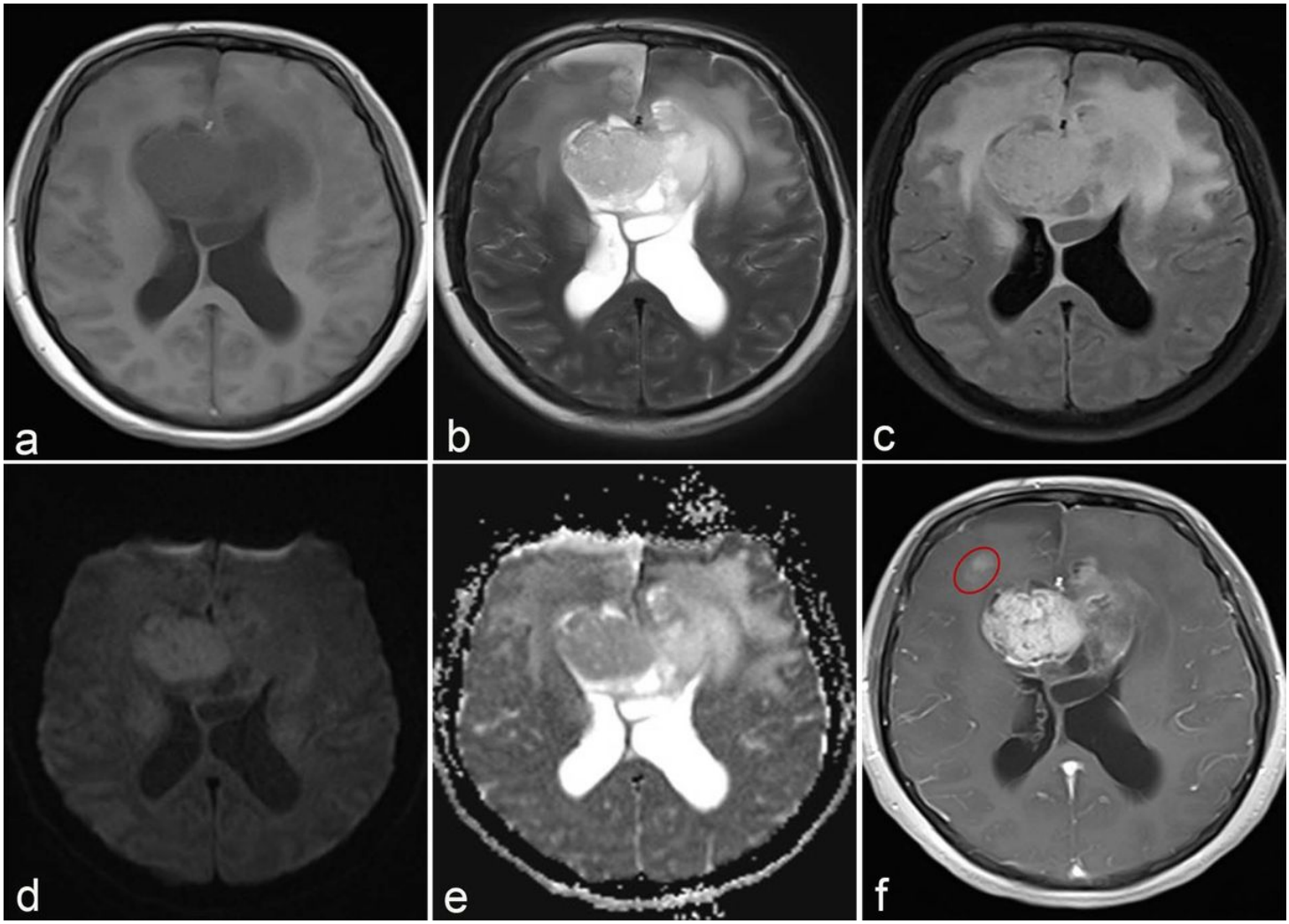

Figure 1

Representative MR imaging of case 6 showing co-location tumor. (a-c) Conventional MRI demonstrates a solid with cystic mass involves bilateral frontal lobes and corpus callosum. The solid part shows notable restricted diffusion on DWI (d) and decreased ADC value (e). (f) T1WI with contrast agent reveals mild enhanced low-grade astrocytoma (red circle) and markedly heterogeneous enhanced eGBM

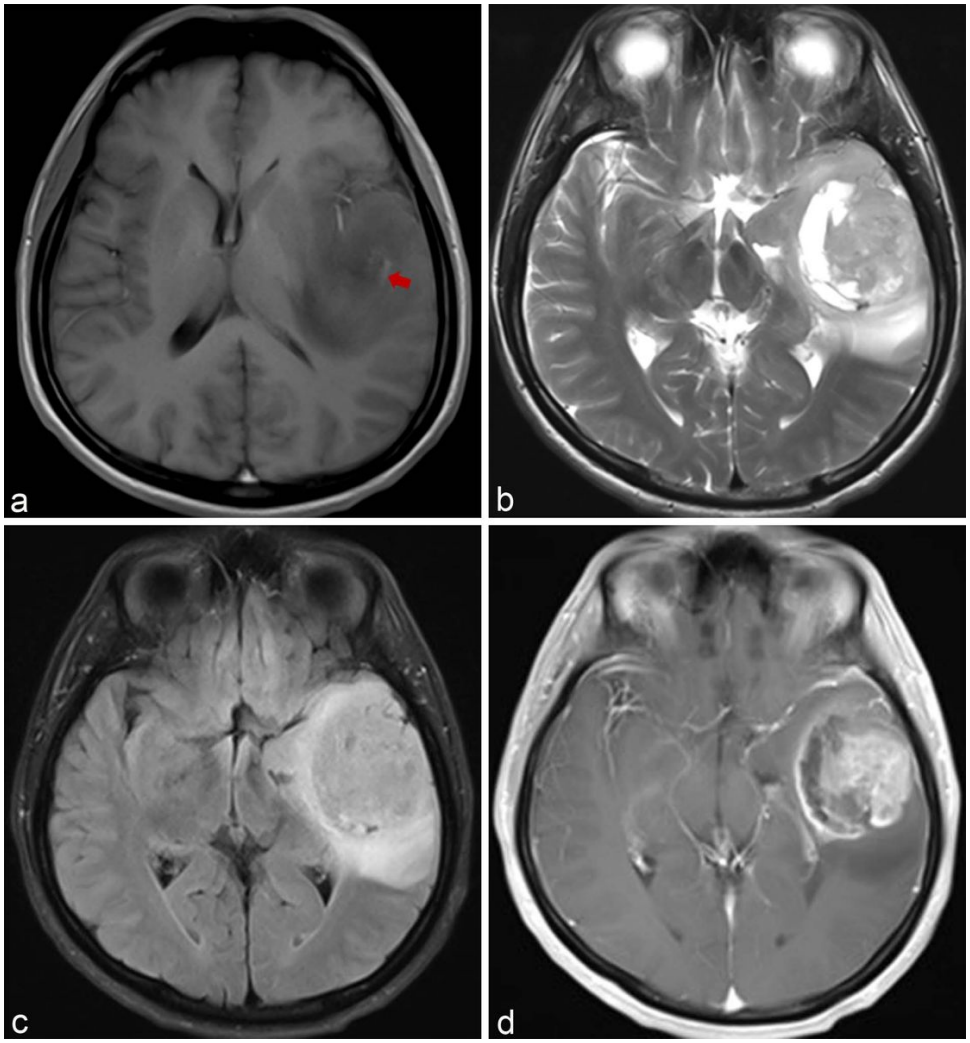

Figure 2

Representative MR imaging of case 1. The tumor sites in left temporal lobe showing hypointensity on T1WI (a), hyperintensity on T2WI (b) and Flair (c). Introtumoral hemorrhage demonstrates hyperintensity on T1WI (red arrow). (d) With contrast agent, in addition to enhancement of solid and cystic wall, adjacent leptomeninge is also enhanced

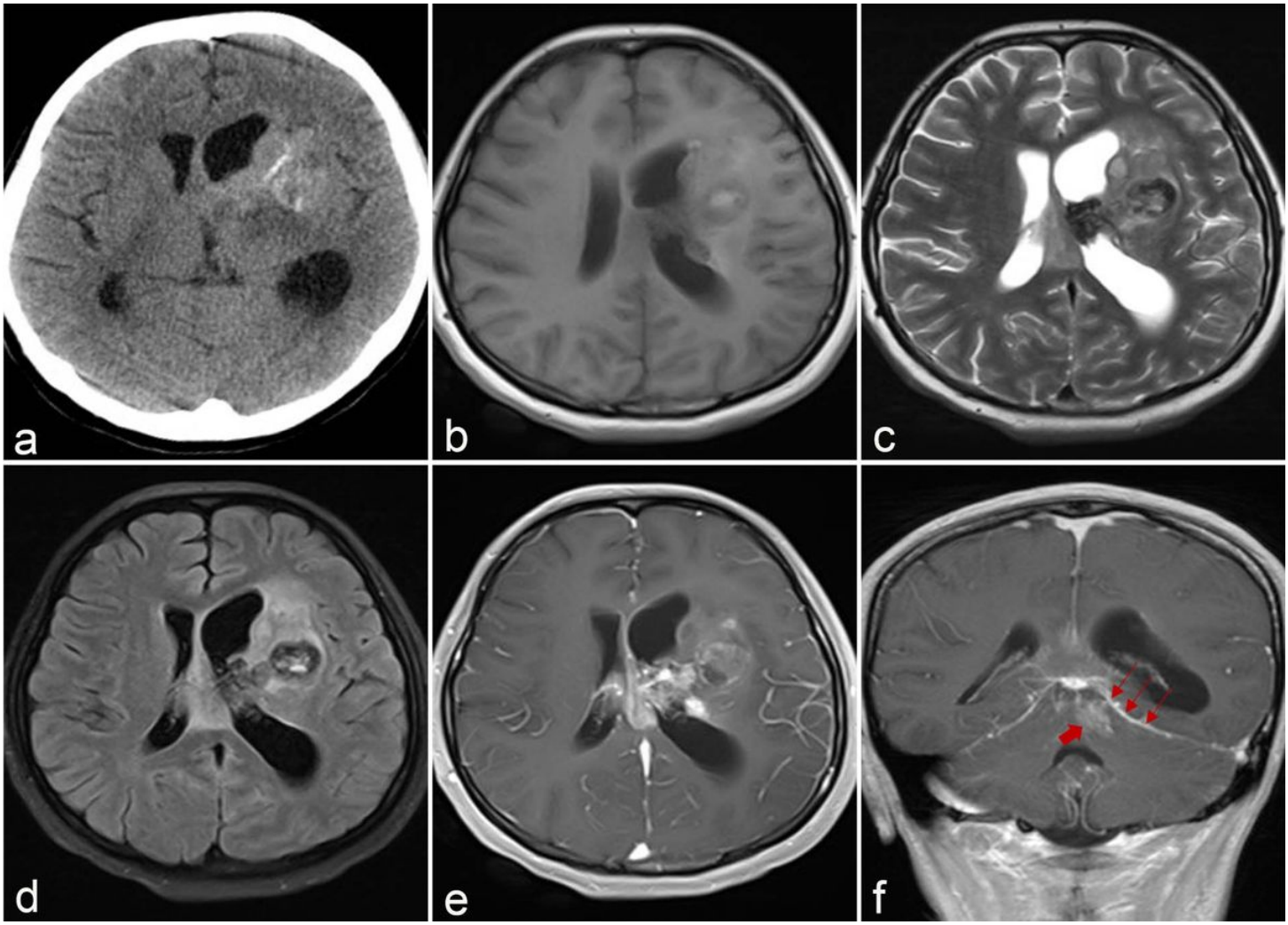

Figure 3

Case 4 showing intratumoral calcium, hemorrhage and dissemination. (a) CT reveals a mass with intratumoral calcium in left basal ganglia. (b-e) T1WI, T2WI, FLAIR and T1WI with contrast agent displays the tumor breaking into left lateral ventricle and involving corpus callosum. Intratumoral hemorrhage demonstrates hyperintensity on T1WI and hypointensity on T2WI. (f) Coronal T1WI with contrast agent reveals the abnormal enhancement in tentorium cerebelli (long arrow) and superior vermis of cerebellum (short arrow)

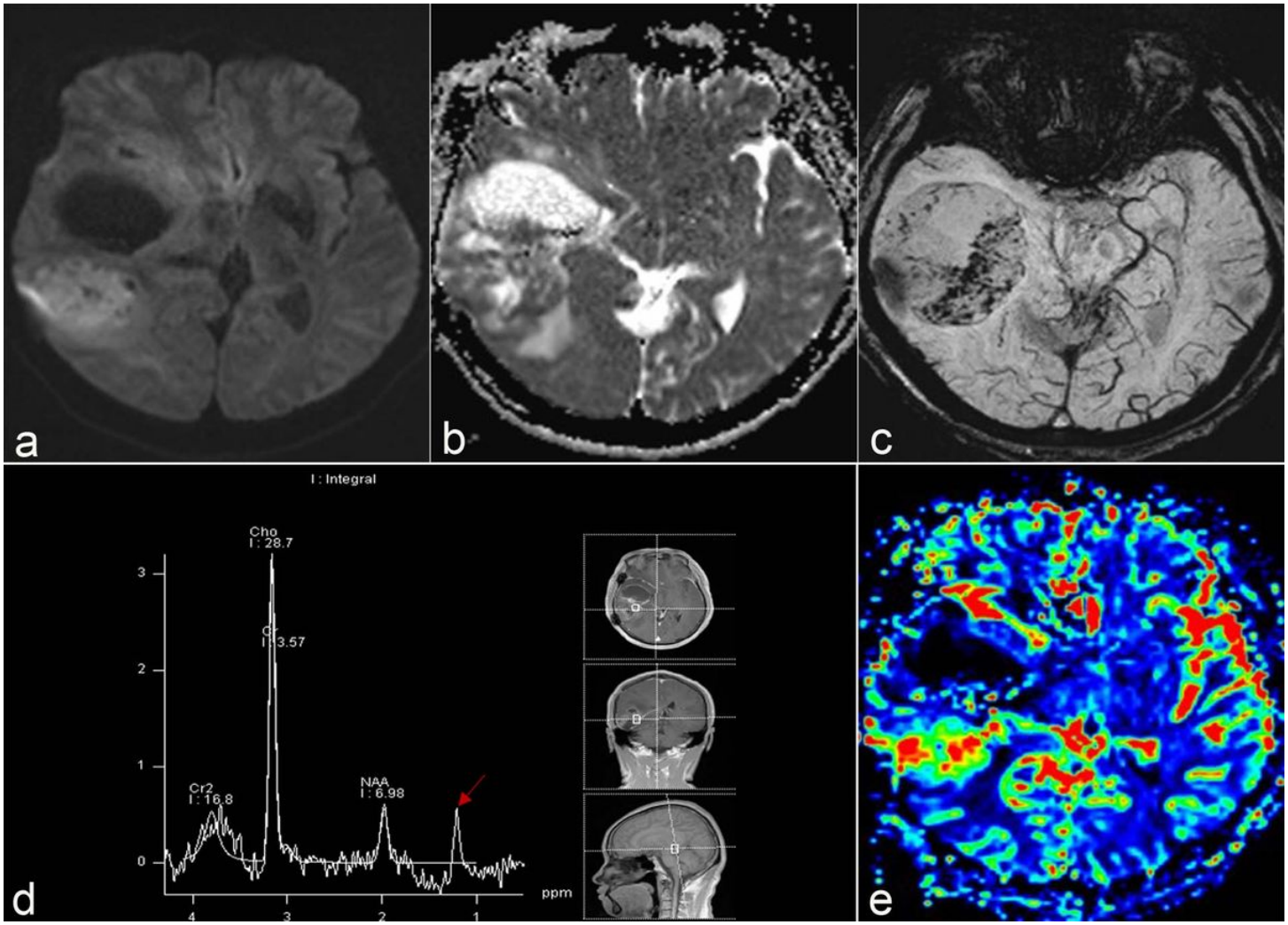

Figure 4

Advanced MRI of case 2. (a, b) Solid part of tumor shows striking restricted diffusion and consequently decreased ADC value. (c) SWI shows multiple dotted or patchy hypointensity within tumor, intratumoral susceptibility signal intensity (ITSS) scores 3. (d) 1H-MRS exhibits decreased NAA, increased Cho and Lac/Lip peak (red arrow) in solid component. (e) CBV map deriving from PWI reveals increased CBV value in solid region

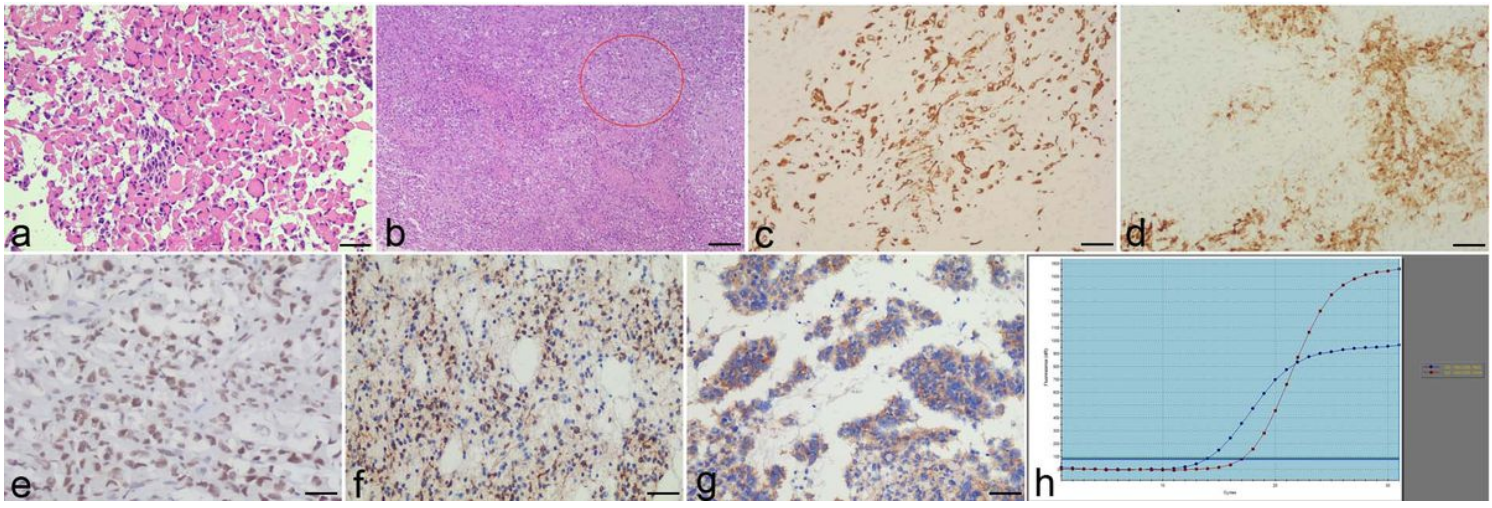

Figure 5

Histopathological characteristics of epithelioid glioblastoma (eGBM). (a, b) HE staining demonstrates discohesive tumor cells with eccentrically positioned nuclei and ample cytoplasm. (b) Another case reveals intratumoral necrosis and local sarcomatoid change (red circle). (c, d) Diffuse and strong positive staining for GFAP and S-100. (e) Retention of nuclear staining of INI-1 is seen in tumor cells. Tumor cells in both low-grade astrocytoma (f) and eGBM (g) region show immunoreactivity for IDH-1. (h) Mutation of BRAF V600E was found in three patients. ×100 (b), ×200 (a, c, d, f, g), ×400 (e)